H-H interaction and structural phase transition in Ti_3SnH_x

Alexei Grechnev,[1,*] Per H. Andersson,[1,2] Rajeev Ahuja,[1] Olle Eriksson,[1] Marie Vennström,[3] and Yvonne Andersson[3]
[1]*Department of Physics, Uppsala University, Box 530, SE-75121, Uppsala, Sweden*
[2]*Swedish Defence Research Agency (FOI), 17290, Stockholm, Sweden*
[3]*Department of Materials Chemistry, Uppsala University, Box 538, SE-75121, Uppsala, Sweden*
(Received 21 September 2001; revised manuscript received 12 July 2002; published 13 December 2002)

The crystalline and electronic structure of metallic Ti_3Sn hydride has been studied by neutron and x-ray diffraction techniques combined with first principles theory (full potential linear muffin-tin orbital and Vienna *ab initio* simulation package projector augmented-wave methods). A phase transition from the hexagonal $D0_{19}$ phase to the cubic $E2_1$ phase upon hydrogenation has been found experimentally and is explained by our calculations. The phase transition is analyzed in terms of the hydrogen-hydrogen interaction which is found to be repulsive. The repulsive H-H interaction is demonstrated to be mainly electronic in origin with an elastic contribution, due to lattice deformation, being an order of magnitude smaller. The origin of the H-H repulsion is found to be the competition between hydrogen-hydrogen and hydrogen-metal bonding. We argue that our analysis can be transferred to nearly any hydrogen-metal system and that it explains the frequently observed repulsive H-H interaction.

DOI: 10.1103/PhysRevB.66.235104 PACS number(s): 71.15.Mb, 61.10.Eq, 61.50.Lt, 71.20.Be

I. INTRODUCTION

The influence of hydrogen on materials properties, when it enters metallic elements, alloys, and compounds, is often dramatic.[1–4] The electronic properties can change from metallic to insulating, and vice versa, as a function of increasing hydrogen content.[5] The material can change chemical properties, structural properties, as well as mechanical properties (ductile to brittle).[6] Other peculiar effects include lattice contraction upon hydrogenation[7] and H ordering.[8] This has caused speculations of using H absorption in metals to tune the materials properties. One of the more practical aspects concerns the use of metal hydrites to store hydrogen as a way to store energy.[9–11] The most obvious obstacle to overcome in using hydrogen as energy storage is the limited amount of hydrogen a given material can absorb, and it seems that the maximum amount of hydrogen that can be stored is 3.6 H atoms per metal atom (in Th).[12] Also the minimal H-H distance in metals is known to be 4 a.u. (so-called 2 Å rule,[13]) although recently a few exceptions to this rule have been found.[14] Part of the reason for this limitation is the repulsive H-H interaction for large concentrations.

The hydrogen-hydrogen interaction in a metal lattice can be divided into elastic and electronic components,[15] where the former is the H-H interaction through the elastic strain of the lattice and the latter includes all other effects. For small H concentrations the elastic component dominates and it is usually attractive.[16] For higher H concentrations the H-H interaction becomes repulsive (see, e.g., Ref. 17). The result of these interactions is that H, when it enters the material, never forms H_2 molecular states but instead exists in an atomic configuration that interacts with the electron states of the host material.

Calculations[18] of the binding energy and binding distance of two H atoms in a uniform electron gas do not quite capture this behavior. For all jellium densities the H atoms attract each other to form an H_2 molecule with equilibrium bond length close to that of the H_2 molecule in vacuum. One could, of course, criticize this conclusion since it is based on a rather crude model, the jellium model, but more realistic calculations on the H-H interactions in metals are sparse, and we conclude that on an electronic structure level there is an unanswered question regarding the H-H interactions in metals.

A microscopic understanding of the repulsive interaction is highly desired, partly in order to find avenues to increase the amount of hydrogen possible to store but also to understand the H interactions in metals in general. In this paper we address this issue by studying the H-H interaction in an ideal model material, Ti_3Sn, an intermetallic compound that, as we will demonstrate below, has structural properties that reflect the H-H interactions in a very clear way.

Ti_3Sn absorbs H readily, forming the compound Ti_3SnH_x, where x ranges from 0 to 1, with hydrogen occupying octahedral voids surrounded by Ti atoms. At a H concentration corresponding to $x=0.7$ the hexagonal $D0_{19}$-type structure (space group $P6_3/mmc$) transforms to the cubic $E2_1$ structure[19–21] (space group $Pm3m$). The two structural forms of Ti_3SnH_x (Fig. 1) are very similar, despite the obvious different symmetries, in a way that quite closely resembles the fcc and hcp crystal structures of the transition metals. For instance, the nearest neighbor Ti-Ti, Ti-Sn, Ti-H and Sn-H distances are almost identical for the two structures

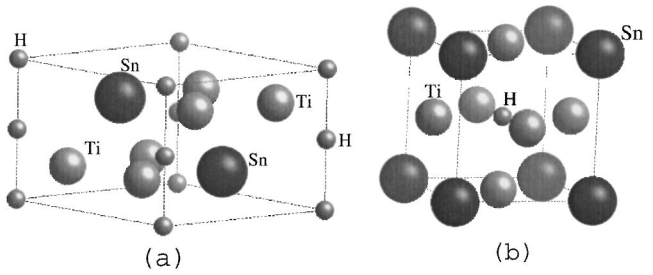

FIG. 1. Unit cell of Ti_3SnH in (a) the $D0_{19}$ structure, (b) the $E2_1$ structure.

TABLE I. Nearest neighbor distances in Ti_3SnH, in a.u., for a volume 460 a.u.^{3}/formula unit.

	Cubic	Hexagonal
Ti-Ti	5.458	5.455
Ti-Sn	5.458	5.455
Ti-H	3.860	3.860
Sn-Sn	7.719	7.719
Sn-H	6.685	6.688
H-H	7.719	4.451

(see Table I), and the most obvious geometrical differences of Ti_3Sn are found for the next nearest neighboring atoms. The most conspicuous difference in atomic geometry of Ti_3SnH_x is the H-H distance which is much larger in the cubic structure, and one may see the structural phase transformation as a way for the material to reduce the influence of the seemingly repulsive H-H interaction. Hence the transformation from hexagonal to cubic crystal structure indicates, as we shall see below, the repulsive interaction in a very clear way. Among other $D0_{19}$-structure intermetallics, Ti_3Al undergoes a similar phase transition,[22] while Ti_3Ga and Ti_3In become amorphous[23] upon hydrogenation.

Our study of Ti_3SnH_x includes both experiment and first principle calculations. Section II explains the crystal structure of Ti_3SnH_x, Sec. III contains details of the first principle calculation, and Sec. IV presents theoretical and experimental results. Finally, the discussion of the results (Sec. V) is followed by the conclusion.

II. CRYSTAL STRUCTURE

Ti_3Sn crystallizes in the hexagonal $D0_{19}$ structure [Fig. 1(a)] (space group $P6_3/mmc$) with unit cell parameters $a=11.1831$ a.u. and $c=9.0047$ a.u.[19,21,24] The unit cell includes two formula units. Ti atoms occupy $6h$ sites $\pm(y,2y,1/4)$, $\pm(2\bar{y},\bar{y},1/4)$ and $\pm(y,\bar{y},1/4)$, with y being close to the ideal value of $y=5/6$. Sn atoms occupy $2c$ sites $\pm(1/3,2/3,1/4)$. Upon hydrogenation the H atoms occupy $2a$ sites (0,0,0) and (0,0,1/2) which are located at the centers of two octahedral voids with six Ti neighbors each.

Ti_3SnH crystallizes in the cubic $E2_1$ structure [Fig. 1(b)] (space group $Pm3m$) with lattice constant $a=7.88$ a.u. and Ti atoms on the $3c$ sites (0,1/2,1/2), (1/2,0,1/2), and (1/2, 1/2, 0); Sn atoms on the $1a$ sites (0,0,0), and H atoms on the $1b$ site (1/2, 1/2, 1/2) which is again the center of the Ti_6 octahedron.

III. DETAILS OF CALCULATIONS

The calculations presented here have been made using the full-potential linear muffin-tin orbital (FP-LMTO) method[25] and the Vienna *ab initio* simulation package (VASP) plane wave code[26] with projector augmented-Wave (PAW) potentials[27] within the local density approximation (LDA) of density functional theory (DFT).

Full structure and volume relaxation have been done for Ti_3SnH_x both in the cubic and hexagonal structures with $x=0$, 0.5, and 1. First the geometry of the unit cell and atomic positions were relaxed using the VASP code with the volume kept constant and equal to 460 a.u.^{3}/ formula unit. Then the relaxed geometry was used to calculate the total energy as a function of volume ranging from 410 to 490 a.u.^{3}/ formula unit, using both VASP and FP-LMTO codes. For the cubic phase with $x=0$ and 1 the unit cell consists of one formula unit while in all other cases (including supercells for $x=0.5$) it includes two formula units.

For the VASP calculations the local density approximation (LDA) has been used. A high plane wave cutoff of 22.7 Ry was used, which is 25% larger than the default cutoff for the hydrogen PAW potential. Monkhorst-Pack k-point mesh with its origin at the Γ point was used. For cubic phases the mesh size was $11\times11\times11$ which gave 56 irreducible k points. For hexagonal phases the mesh size was $11\times11\times9$, providing 80 irreducible k points. For structure relaxation calculations the method of Methfessel and Paxton[28] of order 1 was used for the Brillouin zone integration. For total energy versus volume calculations the modified tetrahedron method of Blöchl et al.[29] was used instead. These choices were made for convenience only since it has been shown that both methods converge with similar speed and accuracy. Tests involving higher values of the cutoff and bigger k-point mesh demonstrated that the values mentioned above give total energy converged to about 10^{-4} Ry. The Ti $3p$ and Sn $4d$ localized bands were treated as valence electrons in the PAW potentials used.

For the FP-LMTO calculations the LDA exchange-correlation functional (von Barth–Hedin parametrization) was used. In the FP-LMTO method the unit cell is divided into nonoverlapping muffin-tin spheres and the interstitial region. The basis functions are linearized muffin-tin orbitals with quantum numbers (n,l,m) and also the tail energy κ^2. The angular part of such basis function is a $Y_{l,m}$ spherical harmonic. The radial part is a numerically calculated function inside the muffin-tin and Hankel or Neumann function in the interstitial region. The potential and the charge density are expanded in spherical harmonics up to $l_{\max}=6$ in the muffin-tin region and in a Fourier series in the interstitial region; therefore there is no shape approximation to the potential or charge density.

All the electrons in the crystal are divided into core, semicore, and valence states. For our calculations the basis set included Ti $3p$ and Sn $4d$ semicore states; Ti $4s,4p,3d$; Sn $5s,5p,5d$ and H $1s,2p,3d$ valence states; all other electron states were treated as core states. We used a double basis set, i.e., two basis functions with different tail energies for each (n,l,m). Namely, $\kappa^2=-0.4,-0.1$ Ry were used for all valence states and $\kappa^2=-0.8,-1.1$ Ry for the semicore states. The k-point meshes included 56 and 120 irreducible k points for cubic and hexagonal structures, respectively, and the Methfessel-Paxton method of order 1 was used for the Brillouin zone integration. For the density of states calculation a larger k point mesh was used: namely 286 irreducible k points for the cubic structure and 395 irreducible k points for the hexagonal structure, and the linear tetrahedron method was used for the Brillouin zone integration.

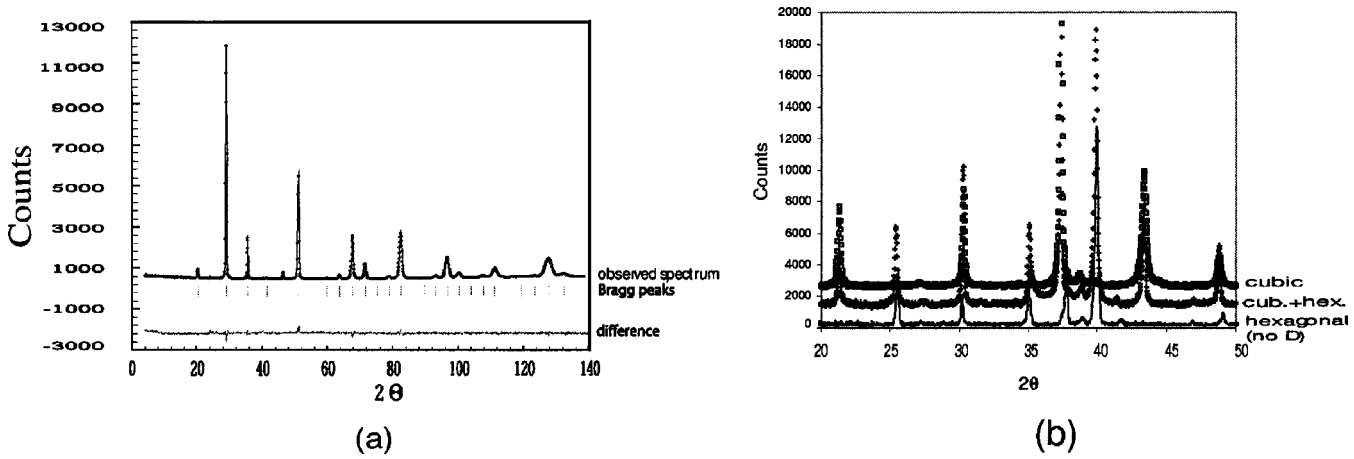

FIG. 2. (a) Observed and calculated neutron powder diffraction profile of cubic Ti_3SnD. (b) X-ray powder diffraction pattern of cubic Ti_3SnD, two phase sample (cubic and hexagonal Ti_3SnD_x), and pure hexagonal Ti_3Sn.

IV. RESULTS

A. Experiment

Ti_3Sn was synthesized by arc melting appropriate amounts of titanium rod (99.99% claimed purity) and tin ingot (99.995% claimed purity) in argon atmosphere. The sample was heat-treated for 7 days at 1173 K in evacuated quarts ampoules. The unit cell of hexagonal Ti_3Sn was determined to be $a=11.1831$ a.u. and $c=9.0047$ a.u., which is in good agreement with previous structure determinations.[24]

The metal hydride phase was obtained by heating the sample to 925 K for 12 h in 70–80 kPa deuterium pressure followed by slow cooling to room temperature. At 70 kPa deuterium pressure the sample contained two phases: an interstitial solid solution and a cubic metal hydride phase. The unit cell dimensions obtained for hexagonal and cubic Ti_3SnD_x were $a=11.1792$ a.u, $c=9.1122$ a.u, and $a=7.8933$, respectively. X-ray powder diffraction pattern of this sample is shown in Fig. 2(b). At increased deuterium pressure a single phase sample with the cubic structure was obtained. The two phase and the single phase samples were measured by neutron powder diffraction techniques and the crystal structure parameters were refined by the Rietveld method. In the two phase sample the hydrogen content was refined to $Ti_3SnD_{0.95}$ and $Ti_3SnD_{0.7}$ in the cubic and hexagonal phases, respectively. The deuterium atoms occupy Ti_6 octahedral positions in both structures. A full account of experimental data has been published elsewhere.[21] The single phase sample contained cubic Ti_3SnD where all Ti_6 octahedral positions are filled with deuterium atom. The observed and calculated neutron diffraction profiles of cubic Ti_3SnD are show in Fig. 2(a) and the structural parameters of the refinement are displayed in Table II.

TABLE II. Results from refinement of Ti_3SnD using the Rietveld method and the program FULLPROF (Ref. 30). Space group $Pm3m$. Unit cell parameter $a=7.8866$ a.u., $R_p=3.74$, $R_{wp}=4.74$, $R_{\exp}=3.74$, $\chi_2=1.60$. $R_{\text{Bragg}}=5.42$, $R_{f\text{-factor}}=5.23$.

Atom	Position	x	y	z	B_{iso}
Ti	$3c$	1/2	0	1/2	0.45(6)
Sn	$1b$	0	0	0	0.42(4)
D	$1a$	1/2	1/2	1/2	1.29(5)

B. Structural stability

As mentioned above, the structural stability of Ti_3SnH_x has been investigated for $x=0$, 0.5, and 1. First the unit cell and geometry have been relaxed with the volume kept constant, then the total energy as a function of volume was calculated. Throughout this section we will report on the energy

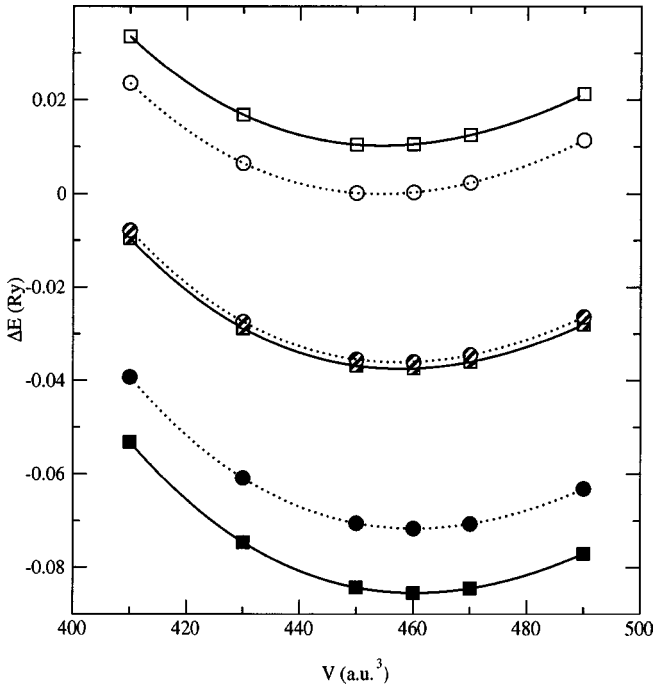

FIG. 3. Heat of formation of Ti_3SnH_x versus volume. $\Delta E \equiv E(Ti_3SnH_x)-(x/2)E(H_2)-E_{\text{hex}}(Ti_3SnH_x)|_{V=V_{\text{eq}}}$. Squares and circles denote cubic and hexagonal phase, respectively. Empty, striped, and filled symbols denote $x=0$, 0.5, and 1 respectively.

TABLE III. Equilibrium volume (a.u.^{3}/formula unit) and calculated bulk modulus (GPa).

	V (exp)	V (FP-LMTO)	V (VASP)	B (VASP)
cub, $x=0$		456.97	454.55	132.02
cub, $x=0.5$		460.31	457.75	137.66
cub, $x=1$	491.8	462.57	460.33	142.56
hex, $x=0$	487.6	456.46	454.27	135.27
hex, $x=0.5$		459.10	457.52	139.47
hex, $x=1$		461.72	460.18	142.75

obtained from the VASP method, although similar calculations were also made with the FP-LMTO method, with only marginal differences between the two methods.

Figure 3 shows the calculated cohesive energy of the cubic and hexagonal phases as function of volume for $x=0$, 0.5, and 1. This was done in the following way. First, the total energy $E(Ti_3SnH_x)$ was calculated. We then calculated the heat of formation of Ti_3SnH_x with respect to the H_2 molecules as

$$\Delta E = E(Ti_3SnH_x) - \frac{x}{2}E(H_2) - E_{hex}(Ti_3SnH_x)|_{V=V_{eq}}, \quad (1)$$

where the total energy of the H_2 molecule has been calculated in the same way as for Ti_3SnH. We used the same PAW potential for hydrogen and the same energy cutoff as for Ti_3SnH_x. For the H_2 calculation, the lattice geometry was a cubic supercell, with a large lattice constant that guarantees small intermolecular interactions (chosen to be 37.8 a.u). The k point mesh included 18 irreducible k points. The convergence of the total energy to an order of 10^{-5} Ry with respect to lattice constant and the k-point mesh has been achieved. The bond length was found to be 1.4495 a.u.

The calculated values of ΔE for the cubic and hexagonal phase as a function of volume are shown for different values of x (Fig. 3). The smooth curves were obtained by fitting to the Murnaghan equation of state. The same equation of state was then used to calculate the equilibrium values of the total energy, volume, and bulk moduli (listed in Table III). From Fig. 3 we note that the energy of Ti_3SnH_x is lower than the total energy of Ti_3Sn and $x/2$ H_2 gas molecules. This means that Ti_3SnH_x is indeed a stable hydride at low temperature. The calculated volume of cubic and hexagonal Ti_3SnH_x is essentially identical for the same x. The difference between calculated and experimental volume is the normal LDA effect. The calculated volume expansion from $x=0$ to $x=1$ is equal to 1.3%, as compared to the experimental value of 0.86%. The values of the c/a ratio from the geometry relaxation are presented in Table IV, together with the lattice spacings a and c. One can see that the c/a ratio for hexagonal Ti_3SnH_x grows upon hydrogenation, and the volume expansion occurs mainly due to the increasing value of c, with a being nearly constant.

TABLE IV. Lattice translation vectors a and c (a.u.) and c/a ratio as found from VASP-PAW calculations.

	a	c	c/a
cub, $x=0$	7.688835		1
cub, $x=0.5$	7.642370	7.837404	1.02552
cub, $x=1$	7.721288		1
hex, $x=0$	10.935488	8.772777	0.80223
hex, $x=0.5$	10.949734	8.812565	0.80482
hex, $x=1$	10.927010	8.900705	0.81456

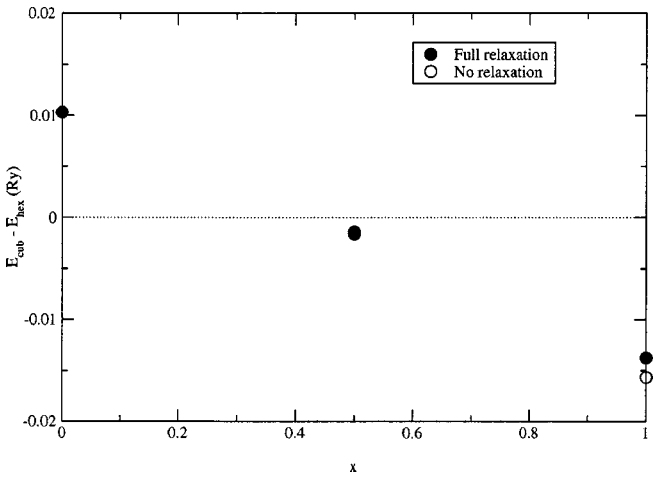

FIG. 4. Energy difference between cubic and hexagonal structures of Ti_3SnH_x as a function of x.

In Fig. 4 we show the energy difference between the cubic and hexagonal phases, as a function of x. One may observe from the figure that for x about 0.5 the theoretical calculations yield the cubic phase to be stable over the hexagonal phase. These results are in agreement with our experimental observations, where it is found that Ti_3Sn absorbs H_2 in an exothermal way and that the cubic phase becomes stable at x larger than 0.7. This experimental finding was also reported in Ref. 19. The often discussed elastic hydrogen-hydrogen interaction can manifest itself in stochiometric phases only as a volume expansion or a change of the lattice geometry. To check if elastic effects are important for the structural phase transition in Ti_3SnH_x, we calculated the total energy of cubic and hexagonal Ti_3SnH_x, for $x=0.5$ and 1, with the equilibrium volume and the unit cell geometry exactly the same as for Ti_3Sn (without H). The results are shown with empty symbols on Fig. 4. One may notice that the elastic effects give a contribution to the energy difference between the cubic and hexagonal phase that is about an order of magnitude smaller than the remaining (electronic) contribution. Therefore, in the rest of the paper we ignore the elastic effects completely and analyze the phase transition only in terms of the electronic structure.

C. Density of states

The calculated density of states (DOS) and partial density of states (PDOS) of the cubic and hexagonal phases of Ti_3Sn, both with and without H ($x=0$ and 1), are presented in Fig. 5. Upon hydrogenation a localized H s-like band ap-

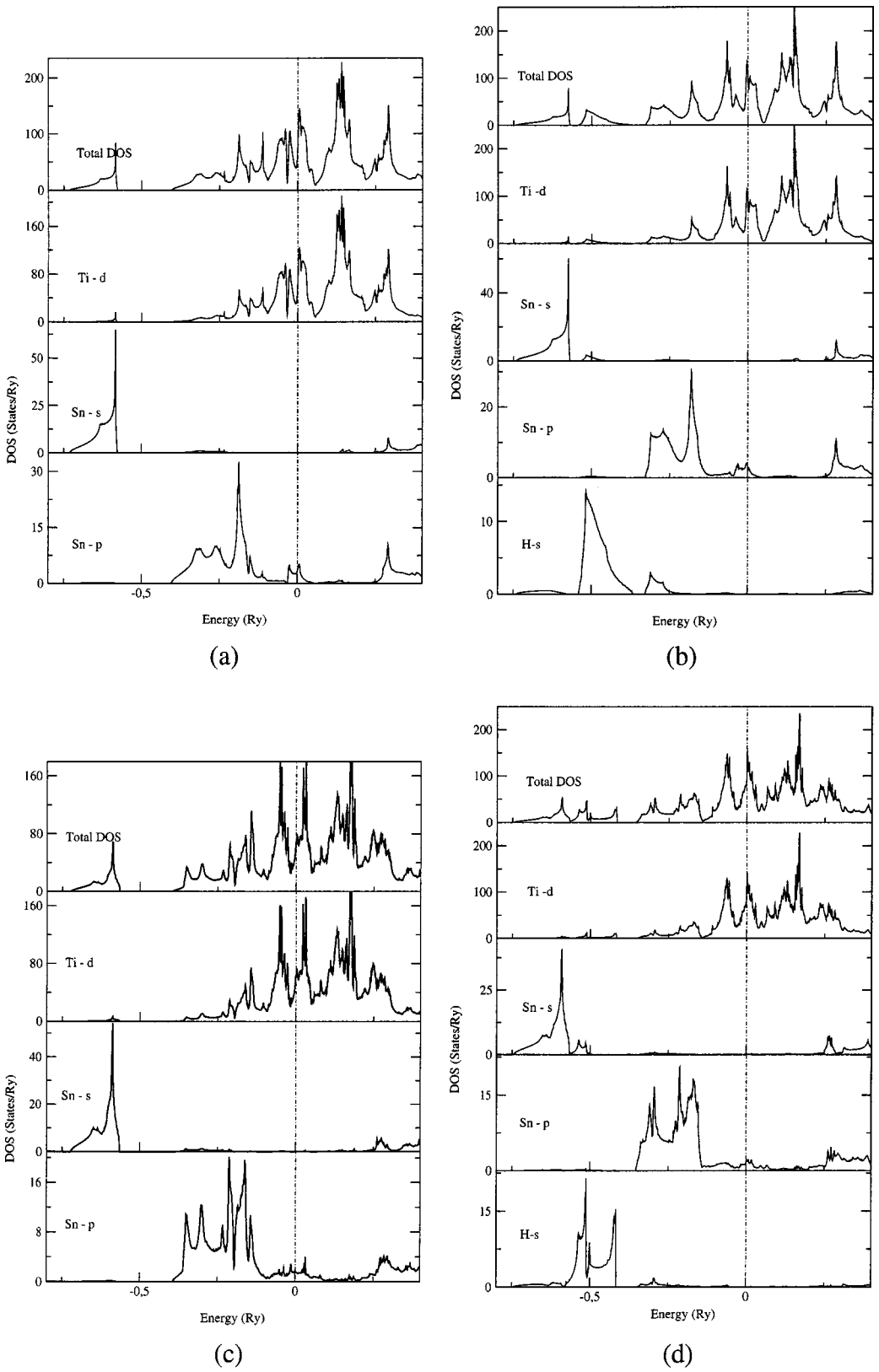

FIG. 5. Partial density of states of (a) cubic Ti_3Sn, (b) cubic Ti_3SnH, (c) hexagonal Ti_3Sn, (d) hexagonal Ti_3SnH. The Fermi level is marked by a dashed-dotted line. The volume is 457 a.u.^{3} for $x=0$ (a,c) and 462 a.u.^{3} for $x=1$ (b,d). Note the different scale of the y axis for different PDOS components.

pears some 0.5 Ry below the Fermi level, between the valence band and the Sn *s*-like band (at ≈ -0.7 Ry).

From the PDOS curves one can conclude that the H-induced feature at 0.5 Ry below E_F has less than 50% H *s* character, with the rest coming from metal states, mainly Ti *d* and Sn *s* states. Therefore hydrogen is not just adding one electron to the valence band (in a rigid band, metallic picture), neither does it form a localized H^- band (in an ionic picture). Instead there is a strong covalent bonding between H atoms and its Ti nearest neighbors, and a hybrid localized band is formed.

Although the valence band for $x=1$ contains one electron less than for $x=0$, the influence of the H atoms seems not very dramatic, at least not around the Fermi level (E_F), both for the cubic and hexagonal phase. The general structures in the DOS around E_F are only marginally modified when H enters the material, with the Fermi level being shifted slightly, making the DOS at the Fermi level somewhat higher for both phases. Of the two phases one may notice a larger Fermi level shift for the hexagonal phase. From this we conclude that the traditional explanation of a certain structure being stable over another, due to modifications in the DOS around E_F, e.g., a formation of a pseudogap close to E_F,[31] cannot explain the observed hexagonal to cubic phase transition.

The bonding of the H 1*s* states with the valence states of Ti_3Sn pushes the bottom of the valence states up in energy with a small amount. However, the most important observation regarding the interaction between the H 1*s* states and the valence states of Ti_3Sn is the strong hybridization with the Ti 3*d* states. This can be seen in Fig. 5(b), since Ti 3*d* states are located in the same energy region as the H 1*s* states (0.5 Ry below E_F). As a result the Ti 3*d* states, which in the unhydrogenated phase are occupied in the region from E_F and 0.4 Ry below, can in the hydrogenated phase lower their energy substantially since they occupy states from E_F and 0.6 Ry below, a fact that is consistent with the exothermic formation of Ti_3SnH.

D. Band filling vs pair potentials

The structural stability of solid state systems can be analyzed semiempirically. One method is to divide the total energy into a term which depends on electron density, but not on the crystal structure, and the sum of all pair-potential contributions (see, e.g., Ref. 32). Alternatively, the structural stability can be analyzed via the filling of the valence band DOS, since it has been shown that formation of pseudogaps in the DOS can favor a certain structure.[31] In addition the so called structural energy difference theorem[32] builds upon such an analysis. In this section we try and contrast these models for the structural stability of Ti_3SnH_x.

From the DOS curves we know that hydrogen in Ti_3SnH actually creates a new feature of hybrid hydrogen-metal character, indicating strong covalent bonding between hydrogen and the metal. The new localized band contains two electrons while the H atom adds only one electron to the system. Therefore, the valence band (not counting the feature at 0.5 Ry below E_F) actually loses one electron rather than gains one. To check the relative importance of band-filling effects versus pair potential contributions to the structural phase transition, we first investigated how the structural stability of Ti_3Sn (without hydrogen) depend on the band filling. In order to do that, we used the virtual crystal approximation (VCA) implemented in the FP-LMTO code. First, we replaced Ti ($Z=22$) atoms in Ti_3Sn with VCA atoms ($Z=22+1/3$) and investigated the structural stability of the system. Such a system has the same number of electrons as Ti_3SnH, if one considers a simplifying model where the H atom donates one electron to a rigid DOS of Ti_3Sn. As a result of the *d*-shell filling, the equilibrium volume decreased by -5.5%. The energy difference $E_{\mathrm{cub}}-E_{\mathrm{hex}}$, however, appeared to be equal to 12 mRy, which is very close to the value of 14 mRy for Ti_3Sn. We also performed a VCA calculation with $Z=22-1/3$ atoms. Such a system has the same number of electrons in the valence band as Ti_3SnH, if one considers a simplifying model where the H atom accepts one electron from a rigid DOS of Ti_3Sn. In that case the volume expands by 6.7% and $E_{\mathrm{cub}}-E_{\mathrm{hex}}=11$ mRy. From this analysis we conclude that the phase stability, $E_{\mathrm{cub}}-E_{\mathrm{hex}}$, is almost independent on filling of the valence band (if one excludes the feature at 0.5 Ry below E_F), and the phase transition should instead be explained in terms of pair potentials.

In the pair potential model, the dependence of $E_{\mathrm{cub}}-E_{\mathrm{hex}}$ with respect to x should be completely attributed to the H-H pair potential, since, as stated above, all other interactions are the same for the cubic and hexagonal structures. It is convenient therefore to write the total energy as

$$E=E_{\mathrm{M}}+\sum_i E_{\mathrm{HM}}(\mathbf{R}_i)+\frac{1}{2}\sum_{ij} V_{\mathrm{HH}}(\mathbf{R}_i-\mathbf{R}_j), \qquad (2)$$

where $E_{\mathrm{HM}}(\mathbf{R}_i)$ describes the interaction of hydrogen atom *i* with the metal sublattice, $V_{\mathrm{HH}}(\mathbf{R}_i-\mathbf{R}_j)$ is the pair interaction between hydrogen atoms *i* and *j*, and E_M includes the electron density term and all metal-metal interactions:

$$E_{\mathrm{M}}=\Phi(\rho)+\frac{1}{2}\sum_{i,j\in M} V_{\mathrm{MM}}(\mathbf{R}_i,\mathbf{R}_j). \qquad (3)$$

To investigate the H–H interaction, we calculated H–H pair potentials directly using supercells with displaced H atoms in a rigid Ti_3Sn matrix (described below). A similar approach has been applied in Ref. 33 to several MH_2 and $ZrM_2H_{1/2}$ systems, where M stands for transition metal.

The atomic configurations used for this purpose are shown on Fig. 6. In all three cases the unit cell of cubic Ti_3SnH is doubled along the *z* direction to include two formula units. The H atoms are displaced along the [110] direction, because this is the direction connecting different octahedral voids with no metal atoms in between. This geometry allows us to investigate the H-H interaction for a wide range of H-H distances. The reference configuration [Fig. 6(a)] keeps the H-H distance constant and equal to the lattice constant $a=7.721$ a.u. If, for this geometry, we neglect the H-H interactions at distances larger than or equal to *a*, then Eq. (2) becomes

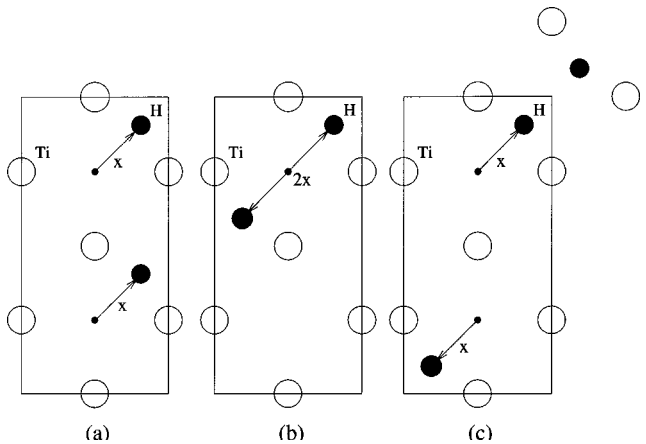

FIG. 6. Geometrical configurations of two hydrogen atoms displaced along the [011] direction. The unit cell is shown for the configurations (a) reference (b) hydrogen atoms centered on a 1*b* (Ti_6 octahedron) site and (c) hydrogen atoms entered on a 3*d* (Ti_4Sn_2 octahedron) site. The crystal structure is cubic and shown for a cut spanned by the vectors [001] and [010]. The dot shows the 1*b* site (center of the Ti_6 octahedral void).

$$E_{\mathrm{ref}}=E_{\mathrm{M}}+E_{\mathrm{HM}}(\mathbf{R}_1)+E_{\mathrm{HM}}(\mathbf{R}_2), \tag{4}$$

where $\mathbf{R}_{1,2}$ are positions of the hydrogen atoms and the energy is defined per unit cell (two formula units). The configurations shown on Fig. 6(b,c) have a pair of H atoms centered on an 1*b* site (at the center of a Ti_6 octahedron) and on a 3*d* site (center of a Ti_4Sn_2 octahedron), respectively. If only the H-H interaction within the pair is taken into account, the energy per unit cell in these two cases becomes

$$E=E_{\mathrm{M}}+E_{\mathrm{HM}}(\mathbf{R}_1)+E_{\mathrm{HM}}(\mathbf{R}_2)+E_{\mathrm{HH}}(d), \tag{5}$$

where the H-H distance, *d*, equals $2x$ and $\sqrt{2}a-2x$ for the configurations of Fig. 6(b) and Fig. 6(c), respectively (x is the displacement of the H atom from the 1*b* site).

The total energy for the three configurations in Fig. 6 as a function of x are presented in Fig. 7(a). In both cases a local minimum exists corresponding to a molecular hydrogenlike state of two H atoms at the octahedral void. The H-H distance for this configuration is 1.7 and 1.9 a.u. for 1*b* and 3*d* sites, respectively, which is larger than the 1.4 a.u. distance of the free H_2 molecule. The energy of such a state is higher than that of cubic Ti_3SnH. A similar situation has been observed for hydrogen in bulk palladium[34,35] and titanium.[36]

The H-H pair potential can now be calculated from Eqs. (5) and (4) as

$$V_{\mathrm{HH}}(d)=E(x)-E_{\mathrm{ref}}(x). \tag{6}$$

The calculated V_{HH} curves for a H-H pair centered on 1*b* and 3*d* sites are presented in Fig. 7(b). Both pair potentials have the same general structure. At short range there is strong repulsion between the H atoms, similar to that of an H_2 molecule. For larger distances the attraction caused by a covalent H-H bonding dominates. The position of the minimum is about 3 and 2.2 a.u. for the H-H pair centered on the 1*b* and 3*d* sites, respectively. This is much larger than the distance of an H_2 molecule (1.4 a.u.). This is also larger than the equilibrium H-H distances of Fig. 7(a) (1.7 and 1.9 a.u., see above), which minimize the total (H-metal plus H-H) potential seen by an H atom. The reason for the difference is that the hydrogen-metal potential [Fig. 7(a)] has minimums at 1*b* and 3*d* sites with a potential barrier in between. If two H atoms are centered at an octahedral void, the hydrogen-metal interactions therefore decreases the H-H distance.

From an inspection of the curve depicting the H-H interaction [Fig. 7(b)] it is tempting to conclude that this interaction is a superposition of the ''normal'' contribution from the H-atoms, e.g., as calculated in a jellium host,[18] and a repulsive component. The former contribution is the balance of the formation of the bonding molecular H_2 orbital and the

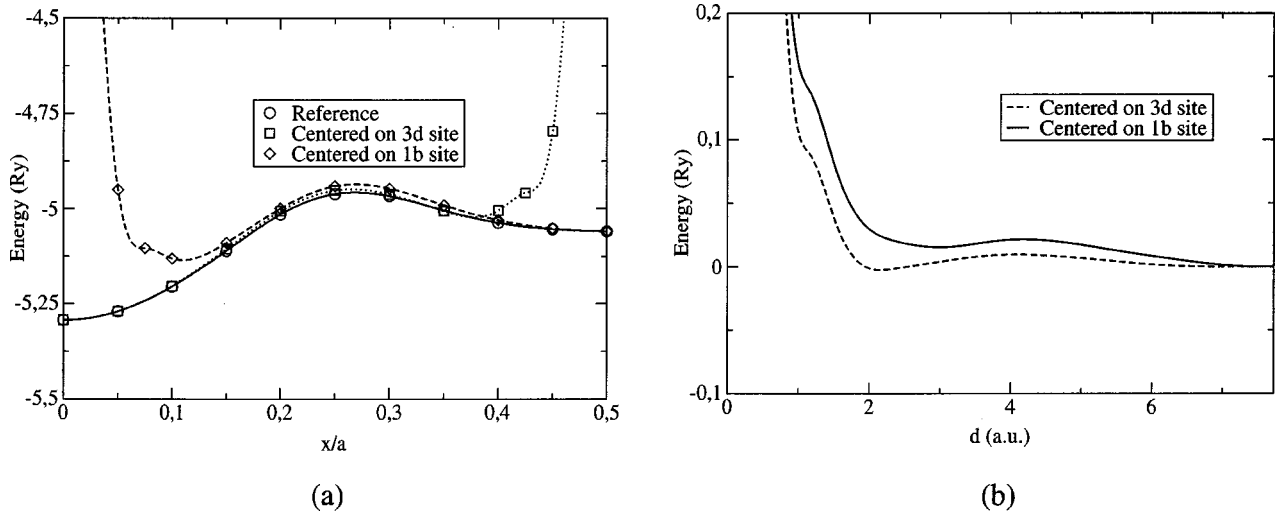

FIG. 7. (a) Total energy for the three H configurations along the [011] direction as function of the displacement x from the 1*b* site. The curve labeled 'Reference' corresponds to the geometry in Fig. 6(a). (b) H-H pair potentials in the [011] direction. The solid curves are given by the cubic splines.

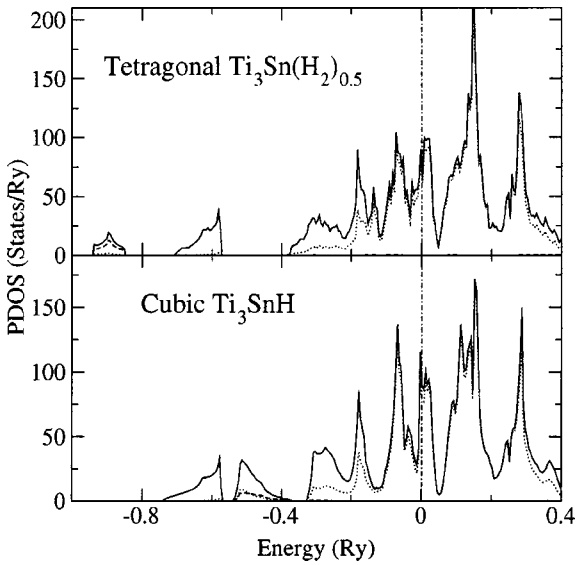

FIG. 8. Partial density of states of cubic Ti_3SnH and $Ti_3Sn(H_2)_{0.5}$ for a volume of 460 a.u.^{3}/formula unit. Solid curve, total DOS; dashed, H 1*s*; dotted, Ti 3*d*. The Fermi level is at zero energy (marked by a dashed-dotted line).

overlap repulsion, which alone would result in a bond distance of 1.4 a.u. The origin of the repulsive component will be discussed below.

The calculated $V_{HH}(d)$ allows us to estimate the energy difference of Ti_3SnH, $E_{cub}-E_{hex}$, using the pair potential model. We only take into account the strongest interaction, namely the interaction of an H atom in hexagonal Ti_3Sn with its two H neighbors and obtain

$$(E_{cub}-E_{hex})_{Ti_3SnH}=(E_{cub}-E_{hex})_{Ti_3Sn}-V_{HH}(d). \quad (7)$$

Using $d=4.451$ a.u. (the H-H distance in the hexagonal Ti_3SnH), the obtained estimates of $(E_{cub}-E_{hex})_{Ti_3SnH}-(E_{cub}-E_{hex})_{Ti_3Sn}$ are -21 mRy and -9 mRy for the H-H centered on 1*b* and 3*d* sites, respectively. This should be compared to the value -24 mRy from the direct total energy calculation. Therefore, the pair potential model is in qualitative agreement with the total-energy calculation, with the pair potential of the H-H pair centered on the 1*b* site giving much better agreement than the one centered on the 3*d* site. The latter result is expected, since H atoms in both cubic and hexagonal Ti_3SnH have Ti nearest neighbors and no Sn nearest neighbors. Therefore the pair potential of a H-H pair centered on the 1*b* site (Ti_6 octahedron) should be more appropriate to describe the phase stability than the 3d site (with the H-H pair centered on the Ti_4Sn_2 octahedron).

V. DISCUSSION

In order to further analyze the nature of the H-H interactions on a microscopic level, connecting it to the electronic structure, we introduce a new superstructure, called the $Ti_3Sn(H_2)_{0.5}$ structure. In this structure we doubled the unit cell of cubic Ti_3SnH along the *z* axis, and put the H-H pair in one octahedron aligned along the [001] direction, leaving the other octahedron empty. The reason for this is that one can then compare differences in the electronic structure between phases when the H-H distance is very large and when it is small. We compare in Fig. 8 the DOS and PDOS of the cubic Ti_3SnH and of the $Ti_3Sn(H_2)_{0.5}$ structure. The DOS and PDOS curves have been calculated with the FP-LMTO method with the H-H distance equal to $d=1.24$ a.u. For Ti_3SnH one again observes the strong Ti 3*d*–H 1*s* hybridization that lowers the total energy of the system and it is the strongest bonding contribution to the formation of Ti_3SnH. The electronic structure of $Ti_3Sn(H_2)_{0.5}$ is different. Here the H 1s states are situated below the Sn s band and the hybridization with all other states in the crystal is weak. The feature at 0.9 Ry below E_F is instead the bonding state of a H_2 molecule in Ti_3Sn that is only weakly influenced by the surrounding Ti and Sn atoms (the antibonding H_2 state is degenerate with the other valence states and is very diffuse). In $Ti_3Sn(H_2)_{0.5}$ there is, as is clear from Fig. 8, very little hybridization between the H states and all other states. The reason that the bonding H state becomes a ''pure'' molecular H_2 state is that the distance between the two H atoms in $Ti_3Sn(H_2)_{0.5}$ is much smaller than all other interatomic distances making the H-H 1s overlap by far the dominant. In addition the energy of the molecular H state is removed from all other electron states, and this reduces the hybridization. The electronic structure of Fig. 8 hence shows a transition from strong attractive H-Ti bonds in Ti_3SnH that result from strongly hybridized Ti-H states, to more or less pure molecular H_2 states in $Ti_3Sn(H_2)_{0.5}$. Since the calculated total energy of Ti_3SnH is lower than that of $Ti_3Sn(H_2)_{0.5}$ we draw the conclusion that the Ti-H bonding is stronger than the H-H bonding.

The analysis presented above shows that the conclusion concerning repulsive H-H interactions in Ti_3Sn, which we used in the sections above to explain the structural transition from hexagonal to cubic, must be modified. It is not so much a question about direct H-H interactions being repulsive, there is always an attractive component due to the formation of a bonding molecular H_2 state. If all other interactions were removed, this would always lead to a bonding H_2 molecule in the metal. However, moving two H atoms closer weakens the strong Ti-H bond. Effectively this shows up as a repulsive H-H interaction. This mechanism is crucial for H-H distance above approximately 4 a.u., i.e., exactly the range important for structural phase transition of Ti_3SnH_x.

The crucial quantity for the mechanism described above is the strength of the hydrogen-hydrogen covalent bond. In the spirit of the LCAO description, it can be related to quantities such as hopping and overlap integrals between hydrogen 1*s* atomic orbitals for a given H-H distance *d*. For instance, the overlap integral is equal to 0.7529, 0.1406, and 0.0127 for H-H distances 1.4, 4.451, and 7.719 a.u., respectively (distances corresponding to H_2 molecule, hexagonal Ti_3SnH, and cubic Ti_3SnH). This comparison, although a bit qualitative, shows that the H-H overlap is larger for hexagonal Ti_3SnH and, together with the repulsive H-H interaction, explains the observed structural phase transition.

VI. CONCLUSION

We have analyzed the H-H interaction in Ti_3Sn via a structural phase transition. The most conspicuous geometrical aspect of the observed phase transition is the distance between the H atoms, which is much larger in the cubic phase. As is often the case, the measured structural properties of Ti_3SnH_x are consistent with a repulsive H-H interaction.

Historically, several simple models for the electronic structure of metal-hydrogen systems have been proposed.[15,37] The rigid band (metallic) model of hydrogenation assumes that each H atom simply gives one electron to a rigid valence band of the metal. In this model H atoms contribute mainly to the band-filling term, and the H-H pair potential is given by the Coulomb interaction screened by the (nearly) free electron gas. Other (tight-binding) models assume that an H atom (or an H^- ion) is only weakly influenced by the crystal surrounding and the tight-binding description is appropriate. In the case of Ti_3SnH_x neither of the models is appropriate, due to strong H-Ti covalent bond. Instead, we considered a realistic *ab initio* electronic structure. Our total energy calculations are consistent with the experimental finding.

Further analysis revealed that the phase stability of Ti_3SnH_x is almost independent on band filling and must be analyzed in the terms of H-H pair potentials instead. We have calculated the H-H pair potential directly using the supercell geometry. The calculated pair potentials reproduce the observed structural stability of the system considered. It has also been established that for the presently studied material the H-H interaction is mainly electronic in origin with the elastic effects being unimportant.

It has been found that the H-H interaction is repulsive for the short H-H separation d, becomes attractive for larger d, and for $d>4$ a.u. it becomes repulsive again. The latter region is specific for hydrogen in metals lattice and has no analogy for hydrogen in vacuum or in the uniform electron gas (jellium).

Our electronic structure theory shows that the H-H interaction always has an attractive component caused by the covalent hydrogen-hydrogen bond. However, the large H-H overlap hampers the stronger H-Ti covalent bond and effectively this shows up as a repulsive H-H interaction. The strong dependence of the electronic structure upon the H-H distance is the explanation for why the H-H interaction depends so strongly on distance.

Our picture of H-H interactions and the connection to the electronic structure transfers easily also to other host materials. Since we have identified the origin of the repulsive H-H interaction to be connected to specific aspects of the electronic structure an avenue opens up to control these interatomic interactions with a controlled modification of the electronic structure, something which may be achieved by alloying or by applying an external pressure. Details of such an investigation are however outside the scope of the present work.

ACKNOWLEDGMENTS

Support from the Swedish Science Foundation (VR) and the foundation for strategic research (SSF) is acknowledged. Valuable discussions with B. Hjörvarsson, P. Ravindran, R. Vidya and P. Vajeeston are acknowledged. We are grateful to Dr. J. M. Wills for supplying the FP-LMTO code.

*Electronic address: Alexei.Grechnev@fysik.uu.se

[1] *Hydrogen in Metals*, Vol. 28 of *Topics in Applied Physics*, edited by G. Alefeld and J. Völkl (Springer, Berlin, 1978).

[2] *Hydrogen in Intermetallic Compounds I*, Vol. 63 of *Topics in Applied Physics*, edited by L. Schlapbach (Springer, Berlin, 1988); *Hydrogen in Intermetallic Compounds II*, Vol. 67 of *Topics in Applied Physics*, edited by L. Schlapbach (Springer, Berlin, 1992).

[3] *Metal-Hydrogen System: Fundamentals and Applications*, edited by F. D. Manchester (Elsevier Sequoia, Lausanne, 1990).

[4] Yuh Fukai, *The Metal-Hydrogen System* (Springer-Verlag, New York, 1993).

[5] J.N. Huiberts, R. Griessen, J.H. Rector, R.J. Wijngaarden, J.P. Dekker, D.G. de Groot, and N.J. Koeman, Nature (London) **380**, 231 (1996).

[6] I.R. Harris, J. Less-Common Met. **131**, 245 (1987).

[7] Yan Wang and M.Y. Chou, Phys. Rev. B **49**, 10 731 (1994).

[8] Yan Wang, Shen N. Sun, and M.Y. Chou, Phys. Rev. B **53**, 1 (1996).

[9] A.J. Maeland, A.F. Andresen, and K. Videm, J. Less-Common Met. **45**, 347 (1976).

[10] G. Sandrock, J. Alloys Compd. **293-295**, 877 (1999).

[11] A.J. Maeland, in *Recent Advances in Hydride Chemistry*, edited by R. Poli (North Holland, Amsterdam, to be published).

[12] M.W. Mallet and I.E. Campell, J. Am. Chem. Soc. **73**, 4850 (1951); D.T. Peterson and J. Rexer, J. Less-Common Met. **4**, 95 (1962).

[13] C. Switendick, Z. Phys. Chem., Neue Folge **117**, 89 (1979).

[14] P. Ravindran, P. Vajeeston, R. Vidya, A. Kjekshus, and H. Fjellvåg, Phys. Rev. Lett. **89**, 106403 (2002); P. Vajeeston, R. Vidya, P. Ravindran, H. Fjellvåg, A. Kjekshus, and A. Skjeltorp, Phys. Rev. B **65**, 075101 (2002).

[15] V.G. Vaks and V.G. Orlov, J. Phys. F: Met. Phys. **18**, 883 (1988).

[16] G. Andersson, P. Andersson, and B. Hjörvarsson, J. Phys.: Condens. Matter **11**, 6669 (1999).

[17] Y. Andersson, S. Rundqvist, R. Tellgren, J.O. Thomas, and T.B. Flanagan, J. Solid State Chem. **32**, 321 (1980).

[18] F. Perrot, J. Phys.: Condens. Matter **6**, 431 (1994).

[19] P.S. Rudman, J.J. Reilly, and R.H. Wiswall, Ber. Bunsenges. Phys. Chem. **82**, 611 (1978).

[20] S. Rundqvist, R. Tellgren, and Y. Andersson, J. Less-Common Met. **101**, 145 (1984).

[21] M. Vennström and Y. Andersson, J. Alloys Compd. **330-332**, 166 (2002).

[22] D. Sornadurai, B. Panigrahi, and Ramani, J. Alloys Compd. **305**, 35 (2000).

[23] K. Mori, K. Aoki, and T. Masumoto, J. Alloys Compd. **231**, 29 (1995).

[24] P. Pietrokowsky, J. Met. **4**, 211 (1952).

[25] J.M. Wills, O. Eriksson, M. Alouani, and D.L. Price, in *Electronic Structure and Physical Properties of Solids: The Uses of the LMTO Method*, edited by H. Dreysse (Springer, Berlin, 1998).
[26] G. Kresse and J. Hafner, J. Phys.: Condens. Matter **6**, 8245 (1994).
[27] P.E. Blöchl, Phys. Rev. B **50**, 17953 (1994); G. Kresse, and D. Joubert, *ibid.* **59**, 1758 (1999).
[28] M. Methfessel and T. Paxton, Phys. Rev. B **40**, 3616 (1989).
[29] Peter E. Blöchl, O. Jepsen, and O.K. Andersen, Phys. Rev. B **49**, 16 223 (1994).
[30] J. Rodriguez-Carjaval, FULLPROF, version 2.0 (LLB, Saclay, France, 2001).
[31] P. Ravindran and R. Asokamani, Phys. Rev. B **50**, 668 (1994).
[32] D.G. Pettifor, *Bonding and Structure of Molecules and Solids* (Clarendon Press, Oxford, 1995).
[33] C. Elsässer, S. Schweizer, and M. Fähnle, Mater. Res. Soc. Symp. Proc. **453**, 221 (1997).
[34] X.W. Wang, S.G. Louie, and M.L. Cohen, Phys. Rev. B **40**, 5822 (1989).
[35] Z. Sun and D. Tomanek, Phys. Rev. Lett. **63**, 59 (1989); P.K. Lam and R. Yu, *ibid.* **63**, 1895 (1989).
[36] M.H. Kang and J.W. Wilkins, Phys. Rev. B **41**, 10 182 (1990).
[37] E.J. Wicke, J. Less-Common Met. **101**, 17 (1984).